

# $P_c(4312)^+$ and $P_c(4337)^+$ as interfering $\Sigma_c\bar{D}$ and $\Lambda_c\bar{D}^*$ threshold cusps

S.X. Nakamura,<sup>1,2,\*</sup> A. Hosaka,<sup>3,4</sup> and Y. Yamaguchi<sup>4</sup>

<sup>1</sup>University of Science and Technology of China, Hefei 230026, People's Republic of China

<sup>2</sup>State Key Laboratory of Particle Detection and Electronics (IHEP-USTC), Hefei 230036, People's Republic of China

<sup>3</sup>Research Center for Nuclear Physics, Osaka University, Ibaraki 567-0047, Japan

<sup>4</sup>Advanced Science Research Center, Japan Atomic Energy Agency (JAEA), Tokai 319-1195, Japan

The recent LHCb data on  $B_s^0 \rightarrow J/\psi p\bar{p}$  revealed a new pentaquark-like  $P_c(4337)^+$  structure, while finding no evidence for  $P_c(4312)^+$  discovered earlier in  $\Lambda_b^0 \rightarrow J/\psi pK^-$ . Though puzzling, the data actually offer an important hint to understand the nature of the pentaquark candidates. We develop a model to analyze the  $B_s^0 \rightarrow J/\psi p\bar{p}$  data. We find that a  $\Sigma_c\bar{D}$  one-loop mechanism causes a threshold cusp that fits well the  $P_c(4337)^+$  peak. Also, the  $\Sigma_c\bar{D}$  and  $\Lambda_c\bar{D}^*$  threshold cusps interfere with each other to reproduce an oscillating behavior in the proton helicity angle distribution. These results combined with our earlier analysis on  $\Lambda_b^0 \rightarrow J/\psi pK^-$  indicate that  $P_c(4312)^+$  and  $P_c(4337)^+$  are created by different interference patterns between the  $\Sigma_c\bar{D}$  and  $\Lambda_c\bar{D}^*$  (anomalous) threshold cusps. The proposed scenario consistently explains why the  $P_c(4312)^+$  and  $P_c(4337)^+$  peaks appear in  $\Lambda_b^0 \rightarrow J/\psi pK^-$  and  $B_s^0 \rightarrow J/\psi p\bar{p}$ , respectively, but not vice versa or both.

## I. INTRODUCTION

Since the discovery of  $X(3872)$  [1], we have witnessed many experimental observations of exotic hadron candidates that are not categorized in the conventional constituent quark structures such as  $q\bar{q}$  and  $qqq$ ; see Refs. [2–9] for reviews. Yet, we have not reached a satisfactory understanding of their nature. Many theoretical attempts have been made to interpret the candidates as hadronic molecules [10–39], compact multiquarks [40–48], or hadrocharmonia [49–51]. However, difficulties of these interpretations lie in: (i) We poorly understand hadron interactions and thus formation mechanisms of the exotic hadrons; (ii) Although resonances are expected to appear in different processes, this is often not the case and their appearances seem to be highly process-dependent.

Kinematical effects, (anomalous) threshold cusps in particular, are an interesting alternative mechanism that can create resonancelike structures [52]. They are rather free from the above item (i) since their singular behaviors occur when certain kinematical conditions are satisfied, irrespective of details of dynamics. The kinematical conditions are often satisfied in one process but not in others and, thus, the item (ii) is naturally understood. In this Letter, taking advantage of these characteristics of the kinematical effects, we propose a scenario on how one can consistently explain pentaquark candidates  $P_c$ 's observed in the recently measured  $\Lambda_b^0$  and  $B_s^0$  decay processes.

The pentaquark candidates were first discovered in  $\Lambda_b^0 \rightarrow J/\psi pK^-$  <sup>1</sup> by the LHCb Collaboration [54]. The recent update with  $\sim 10$  times larger statistics found in the  $J/\psi p$  invariant mass ( $M_{J/\psi p}$ ) distribution three

clear peaks that were assigned to pentaquarks called  $P_c(4312)^+$ ,  $P_c(4440)^+$ , and  $P_c(4457)^+$  [55]. To establish  $P_c^+$ 's as hadronic states, their appearances in different processes have been studied [56–62]. However, the current experimental situation is not very supportive in this regard, though higher statistics data in the future might change the situation. For instance, a  $P_c$  search in the GlueX  $J/\psi$  photoproduction cross section measurement ended up with a null result [63]. Moreover, in  $\Lambda_b^0 \rightarrow J/\psi p\pi^-$  data from the LHCb, an enhanced number of events is seen in the  $M_{J/\psi p}$  bin of  $P_c(4440)^+$  while this is not the case for the other  $P_c^+$ 's [64]. Very recent LHCb data on  $B_s^0 \rightarrow J/\psi p\bar{p}$  has made the situation even more complex [65]. Their four-dimensional amplitude analysis found evidence for a new  $P_c(4337)^+$  signal with a 3.1 – 3.7  $\sigma$  significance, while no evidence was found for  $P_c(4312)^+$ . <sup>2</sup>

Recently, one of the present authors showed that the  $P_c(4312)^+$  peak in  $\Lambda_b^0 \rightarrow J/\psi pK^-$  can be formed by an interference between kinematical effects, including a novel double triangle singularity (DTS), and a smooth amplitude [66, 67]. Within this picture, we can explain the absence of  $P_c(4312)^+$  in the other processes since the DTS does not exist and the interference pattern is different. A similar idea can also be applied to the  $P_c(4337)^+$  signal in  $B_s^0 \rightarrow J/\psi p\bar{p}$ .

In this work, we develop a model for  $B_s^0 \rightarrow J/\psi p\bar{p}$  that consists of one-loop [Fig. 1(a)] and direct decay [Fig. 1(b)] mechanisms. The one-loop amplitudes cause threshold cusps in the  $M_{J/\psi p}$  distribution. We demonstrate that the  $\Sigma_c\bar{D}$  threshold cusp develops a structure that fits well the  $P_c(4337)^+$  peak. Furthermore, the  $\Sigma_c\bar{D}$  and  $\Lambda_c\bar{D}^*$  one-loop amplitudes, which are expected to have comparable magnitudes, interfere with each other to create an oscillating behavior in the proton helicity angle

\* satoshi@ustc.edu.cn

<sup>1</sup> We follow the hadron naming scheme of [53]. For simplicity, however,  $\Sigma_c(2455)^{+(++)}$ ,  $\Sigma_c(2520)^{+(++)}$ , and  $J/\psi$  are often denoted by  $\Sigma_c$ ,  $\Sigma_c^*$ , and  $\psi$ , respectively. We also collectively denote  $\Lambda_c$  and  $\Sigma_c$  by  $Y_c$ . Charge indices are often suppressed.

<sup>2</sup> We do not discuss  $P_c(4440)^+$  and  $P_c(4457)^+$  hereafter since they are located (virtually) outside of the phase-space of  $B_s^0 \rightarrow J/\psi p\bar{p}$ .

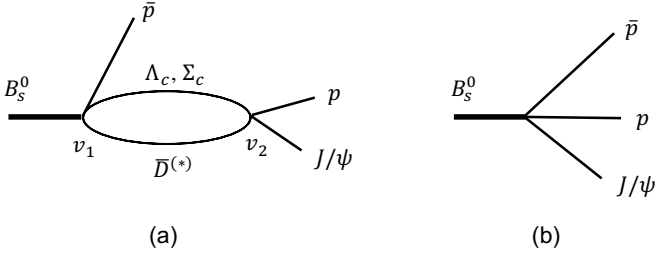


FIG. 1.  $B_s^0 \rightarrow J/\psi p \bar{p}$  mechanisms considered in this work: (a) one-loop; (b) direct decay. Diagrams with charge-conjugated intermediate and final states are also considered.

distribution in a remarkable agreement with the data. With these results, we provide a reasonable explanation why the resonancelike  $P_c(4312)^+$  and  $P_c(4337)^+$  peaks selectively appear in  $\Lambda_b^0 \rightarrow J/\psi p K^-$  and  $B_s^0 \rightarrow J/\psi p \bar{p}$ , respectively.

## II. MODEL

The one-loop mechanisms [Fig. 1(a)] are initiated by  $B_s^0 \rightarrow Y_c \bar{D}^{(*)}(J^P) \bar{p}$  with  $Y_c \bar{D}^{(*)}(J^P) = \Lambda_c \bar{D}^0(1/2^-)$ ,  $\Lambda_c \bar{D}^{*0}(1/2^-)$ , and  $\Sigma_c \bar{D}(1/2^-)$ ;  $J^P$  stands for the spin ( $J$ ) and parity ( $P$ ) of the  $Y_c \bar{D}^{(*)}$  pair. These weak decays would be mainly caused by quark-level mechanisms shown in Figs. 2(a) and 2(b). The  $Y_c \bar{p}$  in Fig. 2(a) could be generated from a decay chain such as  $B_s^0 \rightarrow D^{**} \bar{D}^{(*)}$ ,  $D^{**} \rightarrow Y_c \bar{p}$  with  $D^{**}$  being an excited charmed meson. In this case, a  $D^{**} Y_c \bar{D}^{(*)}$  triangle diagram would contribute to  $B_s^0 \rightarrow J/\psi p \bar{p}$ . However, such triangle diagrams may be simulated by Fig. 1(a) because, with experimentally confirmed charmed mesons, they do not cause triangle singularities. Similarly, the diagram of Fig. 2(b) might induce a  $\bar{Y}_c^{**} Y_c \bar{D}^{(*)}$  triangle diagram that may be simulated by Fig. 1(a).

Another triangle diagram can be drawn from Fig. 1(a) by replacing the contact interaction  $v_2$  with a  $D^{(*)}$ -exchange mechanism. This triangle diagram is similar to initial single pion emission (ISPE) mechanisms that have been used to describe the  $Z_b(10610)$  and  $Z_b(10650)$  structures [68] and the  $Z_c(3900)$  structure [69]. Since the exchanged  $D^{(*)}$ -meson is highly off-shell, this ISPE-like mechanism should be well approximated and included in the one-loop mechanism of Fig. 1(a). The contact interaction  $v_2$  would also include other possible short-range mechanisms such as a quark-exchange.

Regarding the direct decay [Fig. 1(b)], we expect and assume it to be also initiated by the quark diagrams of Figs. 2(a) and 2(b). Thus, the direct decay simulates one-loop mechanisms including heavier  $Y_c \bar{D}^{(*)}(J^P)$  such as  $\Sigma_c \bar{D}^{*}(1/2^-)$ . Meanwhile, one may expect another quark diagram of Fig. 2(c) as a main driver for  $B_s^0 \rightarrow J/\psi p \bar{p}$  [70]. However, the  $p \bar{p}$  pair created in this way must go through a strong final state interaction,

causing a significant  $p \bar{p}$  threshold enhancement [71, 72]. The absence of such enhancement in the LHCb data [65] would indicate that this quark diagram plays a minor role.

Now we present formulas for the one-loop amplitudes. Masses and widths of the particles that contribute to the amplitudes are taken from Ref. [53]. We denote the energy, width, momentum, and polarization vector of a particle  $x$  by  $E_x$ ,  $\Gamma_x$ ,  $\mathbf{p}_x$ , and  $\boldsymbol{\epsilon}_x$ , respectively. The initial  $B_s^0 \rightarrow Y_c \bar{D}^{(*)}(J^P) \bar{p}$  vertices with  $Y_c \bar{D}^{(*)}(J^P) = \Lambda_c \bar{D}^0(1/2^-)$ ,  $\Lambda_c \bar{D}^{*0}(1/2^-)$ , and  $\Sigma_c \bar{D}(1/2^-)$  are given by

$$v_{1a} = c_{\Lambda_c \bar{D} \bar{p}, B_s}^{1/2^-} F_{\Lambda_c \bar{D} \bar{p}, B_s}^{00}, \quad (1)$$

$$v_{1b} = c_{\Lambda_c \bar{D}^* \bar{p}, B_s}^{1/2^-} \boldsymbol{\sigma} \cdot \boldsymbol{\epsilon}_{\bar{D}^*} F_{\Lambda_c \bar{D}^* \bar{p}, B_s}^{00}, \quad (2)$$

$$v_{1c} = c_{\Sigma_c \bar{D} \bar{p}, B_s}^{1/2^-} \left( 1 t_{\Sigma_c} \frac{1}{2} t_{\bar{D}} \left| \frac{1}{2} \frac{1}{2} \right. \right) F_{\Sigma_c \bar{D} \bar{p}, B_s}^{00}, \quad (3)$$

respectively, with complex coupling constants  $c_{Y_c \bar{D}^{(*)} \bar{p}, B_s}^{J^P}$ . The parenthesis is an isospin Clebsch-Gordan coefficient with  $t_x$  being the isospin  $z$ -component of a particle  $x$ . We have used dipole form factors  $F_{ijk,l}^{LL'}$  defined by

$$F_{ijk,l}^{LL'} = \frac{1}{\sqrt{E_i E_j E_k E_l}} \left( \frac{\Lambda^2}{\Lambda^2 + q_{ij}^2} \right)^{2+\frac{l}{2}} \left( \frac{\Lambda^2}{\Lambda^2 + \tilde{p}_k^2} \right)^{2+\frac{l'}{2}}, \quad (4)$$

where  $q_{ij}$  ( $\tilde{p}_k$ ) is the momentum of  $i$  ( $k$ ) in the  $ij$  (total) center-of-mass frame. Unless otherwise stated, we use a common cutoff value  $\Lambda = 1$  GeV in Eqs. (4) and (8) for all the interaction vertices. The subsequent  $s$ -wave interactions for  $\Lambda_c^+ \bar{D}^0(1/2^-)$ ,  $\Lambda_c^+ \bar{D}^{*0}(1/2^-)$ ,  $\Sigma_c \bar{D}(1/2^-) \rightarrow J/\psi p$  are given by separable interactions with coupling

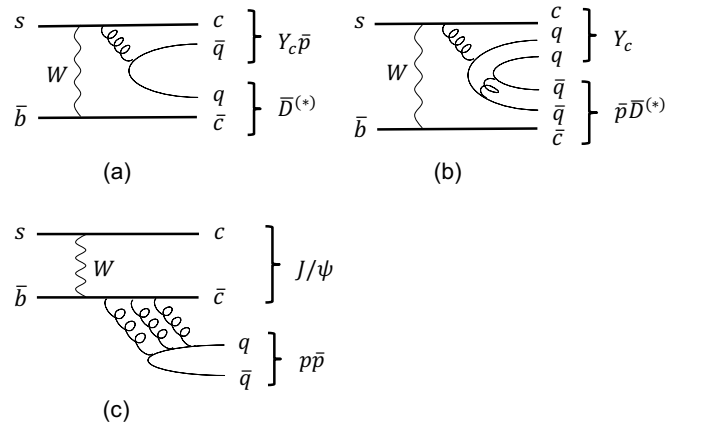


FIG. 2. Possible quark diagrams for (a,b)  $B_s^0 \rightarrow Y_c \bar{p} \bar{D}^{(*)}$  and (c)  $B_s^0 \rightarrow J/\psi p \bar{p}$ ;  $q = u$  or  $d$ .

constants  $c_{\psi p, Y_c \bar{D}^{(*)}}^{J^P}$  as

$$v_{2a} = c_{\psi p, \Lambda_c \bar{D}}^{1/2^-} \boldsymbol{\sigma} \cdot \boldsymbol{\epsilon}_\psi f_{\psi p}^0 f_{\Lambda_c \bar{D}}^0, \quad (5)$$

$$v_{2b} = c_{\psi p, \Lambda_c \bar{D}^*}^{1/2^-} \boldsymbol{\sigma} \cdot \boldsymbol{\epsilon}_\psi \boldsymbol{\sigma} \cdot \boldsymbol{\epsilon}_{\bar{D}^*} f_{\psi p}^0 f_{\Lambda_c \bar{D}^*}^0, \quad (6)$$

$$v_{2c} = c_{\psi p, \Sigma_c \bar{D}}^{1/2^-} \left( 1 t_{\Sigma_c} \frac{1}{2} t_{\bar{D}} \left| \frac{1}{2} \frac{1}{2} \right. \right) \boldsymbol{\sigma} \cdot \boldsymbol{\epsilon}_\psi f_{\psi p}^0 f_{\Sigma_c \bar{D}}^0, \quad (7)$$

with form factors

$$f_{ij}^L = \frac{1}{\sqrt{E_i E_j}} \left( \frac{\Lambda^2}{\Lambda^2 + q_{ij}^2} \right)^{2+(L/2)}. \quad (8)$$

The one-loop amplitudes including  $Y_c \bar{D}^{(*)}(J^P)$ , denoted by  $A_{Y_c \bar{D}^{(*)}(J^P)}^{1L}$ , are given with the above ingredients as

$$A_{\Lambda_c \bar{D}(1/2^-)}^{1L} = c_{\psi p, \Lambda_c \bar{D}}^{1/2^-} c_{\Lambda_c \bar{D} \bar{p}, B_s}^{1/2^-} \boldsymbol{\sigma} \cdot \boldsymbol{\epsilon}_\psi \int d^3 p \bar{D} \frac{f_{\psi p}^0 f_{\Lambda_c \bar{D}}^0 F_{\Lambda_c \bar{D} \bar{p}, B_s}^{00}}{W - E_{\Lambda_c} - E_{\bar{D}} + i\epsilon}, \quad (9)$$

$$A_{\Lambda_c \bar{D}^*(1/2^-)}^{1L} = 3 c_{\psi p, \Lambda_c \bar{D}^*}^{1/2^-} c_{\Lambda_c \bar{D}^* \bar{p}, B_s}^{1/2^-} \boldsymbol{\sigma} \cdot \boldsymbol{\epsilon}_\psi \int d^3 p \bar{D}^* \frac{f_{\psi p}^0 f_{\Lambda_c \bar{D}^*}^0 F_{\Lambda_c \bar{D}^* \bar{p}, B_s}^{00}}{W - E_{\Lambda_c} - E_{\bar{D}^*} + i\epsilon}, \quad (10)$$

$$A_{\Sigma_c \bar{D}(1/2^-)}^{1L} = c_{\psi p, \Sigma_c \bar{D}}^{1/2^-} c_{\Sigma_c \bar{D} \bar{p}, B_s}^{1/2^-} \boldsymbol{\sigma} \cdot \boldsymbol{\epsilon}_\psi \sum_{\text{charge}} \left( 1 t_{\Sigma_c} \frac{1}{2} t_{\bar{D}} \left| \frac{1}{2} \frac{1}{2} \right. \right)^2 \int d^3 p \bar{D} \frac{f_{\psi p}^0 f_{\Sigma_c \bar{D}}^0 F_{\Sigma_c \bar{D} \bar{p}, B_s}^{00}}{W - E_{\Sigma_c} - E_{\bar{D}} + \frac{i}{2} \Gamma_{\Sigma_c}}, \quad (11)$$

where  $\sum_{\text{charge}}$  indicates the summation over  $\Sigma_c^+ \bar{D}^0$  and  $\Sigma_c^{++} \bar{D}^-$  intermediate states with the charge dependent particle masses;  $W \equiv E - E_{\bar{p}}$ ; the tiny  $\Gamma_{D^*}$  has been neglected. The above expressions are implicitly sandwiched by the spinors of the final  $p$  and  $\bar{p}$ .

The one-loop amplitudes in Eqs. (9)-(11) are further supplemented by  $Y_c \bar{D}^{(*)}$  scattering amplitudes. Here, we use a  $Y_c \bar{D}^{(*)}$  single channel scattering model used in Ref. [66]; see Sec. 2 of the Supplemental Material in Ref. [66] for details. We assume possible coupled-channel and/or multi-loop effects to be absorbed by the coupling constants that are fitted to the data. The  $Y_c \bar{D}^{(*)}$  interaction strengths are fixed such that the scattering lengths<sup>3</sup> are  $a \sim 0.5$  fm (attractive) for  $\Sigma_c \bar{D}$  while  $a \sim -0.2$  fm (repulsive) for  $\Lambda_c \bar{D}^*$  as in Ref. [66]. Regarding  $\Lambda_c \bar{D}$  not considered in Ref. [66], we use a scattering amplitude of  $a \sim -0.2$  fm as the fit prefers a repulsion. The one-loop amplitudes create threshold cusps in the  $M_{J/\psi p}$  spectrum that become significantly sharper [less sharp] as the  $Y_c \bar{D}^{(*)}$  interactions are more attractive [repulsive] [73]. However, the positions of the cusps are not very sensitive to the  $a$  values since they are determined by the kinematical effects.

For the direct decay amplitude, we employ the following one for  $p J/\psi(1/2^-)$  partial wave as

$$A_{\text{dir}} = c_{\text{dir}}^{1/2^-} \boldsymbol{\sigma} \cdot \boldsymbol{\epsilon}_\psi F_{p\psi\bar{p}, B_s}^{00}, \quad (12)$$

where  $c_{\text{dir}}^{1/2^-}$  is a coupling constant. This amplitude creates  $J/\psi p \bar{p}$  such that all two-particle pairs are in  $s$ -wave and, therefore, it has a similarity to the non-resonant amplitude used in the LHCb analysis [65].

Our full  $B_s^0 \rightarrow J/\psi p \bar{p}$  decay amplitude also includes the diagrams obtained from Fig. 1 by replacing the intermediate and final particles with their charge-conjugates. The amplitudes for such charge analogous mechanisms are obtained from Eqs. (9)-(12) by replacements  $Y_c \rightarrow \bar{Y}_c$  and  $\bar{D}^{(*)} \rightarrow D^{(*)}$ , and by interchanges  $p \leftrightarrow \bar{p}$ , assuming that the coupling constants do not change. Thus, the Dalitz plot distribution from this model is symmetric with respect to interchanging  $p$  and  $\bar{p}$ . See Appendix B of Ref. [74] for details on how to calculate the Dalitz plot distribution using the presented amplitudes.

### III. RESULTS

Our  $B_s^0 \rightarrow J/\psi p \bar{p}$  model is fitted to the LHCb data for the  $M_{J/\psi p}$  and  $M_{J/\psi \bar{p}}$  distributions and also for the proton helicity angle ( $\theta_p$ ) distribution;  $\cos \theta_p \equiv -\hat{p}_p \cdot \hat{p}_\psi$  with  $\hat{p}_x \equiv \mathbf{p}_x / |\mathbf{p}_x|$  in the  $p \bar{p}$ -at-rest frame. As the LHCb data is the sum of the  $B_s^0$  and  $\bar{B}_s^0$  decays, the data is symmetric with respect to interchanging  $p$  and  $\bar{p}$  under the  $CP$  conservation. Regarding the fitting parameters, each of the one-loop amplitudes [Eqs. (9)-(11)] has an independent complex parameter  $c_{\psi p, Y_c \bar{D}^{(*)}}^{1/2^-} c_{Y_c \bar{D}^{(*)} \bar{p}, B_s}^{1/2^-}$ . The direct decay amplitude [Eq. (12)] also has a coupling constant  $c_{\text{dir}}^{1/2^-}$ . Since the overall normalization and phase of the full amplitude are arbitrary, we totally have six fitting parameters.

A reasonable fit is obtained for the  $M_{J/\psi p}$  and  $M_{J/\psi \bar{p}}$  distributions as shown in Fig. 3(a); the theoretical curves have been smeared with the bin width. By working with the six fitting parameters, we do not find another solution of a comparable quality. Parameter values are given in Table I. We have plotted the results for two models, one with the  $Y_c \bar{D}^{(*)}$  single channel scattering amplitude

<sup>3</sup> The scattering length ( $a$ ) is related to the phase shift ( $\delta$ ) by  $p \cot \delta = 1/a + \mathcal{O}(p^2)$ .

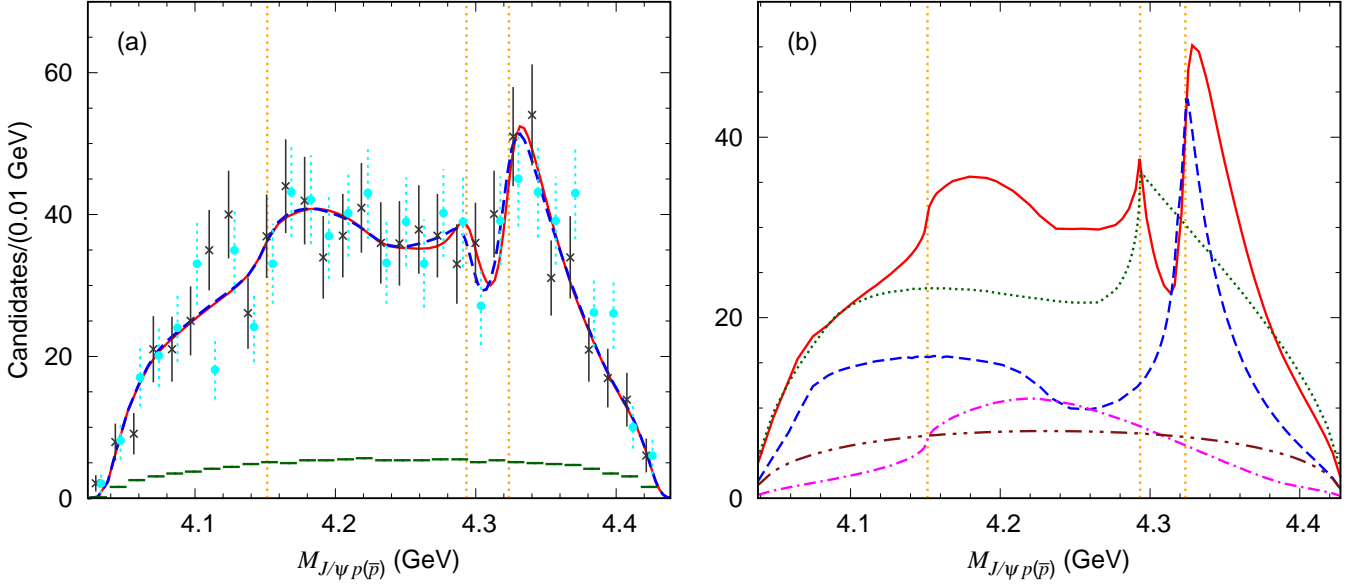


FIG. 3.  $J/\psi p$  and  $J/\psi \bar{p}$  invariant mass distributions for  $B_s^0 \rightarrow J/\psi p \bar{p}$ . (a) Comparison with the LHCb data [65]. The red solid [blue dashed] curve is from the full model with [without] the  $Y_c \bar{D}^{(*)}$  single-channel scattering amplitudes, augmented by experimental background (green histogram) [65] and smeared with the bin width. The dotted vertical lines indicate thresholds for, from left to right,  $\Lambda_c^+ \bar{D}^0$ ,  $\Lambda_c^+ \bar{D}^{*0}$ , and  $\Sigma_c(2455)^{++} D^-$ , respectively. The black crosses (cyan circles) are the  $J/\psi p$  ( $J/\psi \bar{p}$ ) data and are shifted by  $-2$  MeV ( $+2$  MeV) along the  $M_{J/\psi p(\bar{p})}$  axis for better visibility. (b) Contribution from each mechanism. The blue dashed, green dotted, and magenta dash-dotted curves are from the  $\Sigma_c \bar{D}$ ,  $\Lambda_c \bar{D}^*$ , and  $\Lambda_c \bar{D}$  one-loop mechanisms, respectively; the corresponding charge-conjugate  $\bar{Y}_c D^{(*)}$  one-loop is also included in each. The brown dash-two-dotted curve is from the direct decay mechanism. These contributions are coherently summed to give the red solid curve. The curves are not smeared.

included (red solid curve), and the other without (blue dashed curve). As we observe in the figure, the fit quality is not significantly different between the two models. The

TABLE I. Parameter values for our  $B_s^0 \rightarrow J/\psi p \bar{p}$  models. The second (third) column is for the model that includes (does not include) the single channel  $Y_c \bar{D}^{(*)}$  scattering amplitudes. The parameters above (below) the horizontal line are obtained from (not) fitting the LHCb data [65]. The parameters above the horizontal line can be arbitrarily scaled by a common complex overall factor. The last three parameters are  $Y_c \bar{D}^{(*)} \rightarrow Y_c \bar{D}^{(*)}$  interaction strengths defined by Eq. (43) in the Supplemental Material of Ref. [66].

$C_{\psi p, \Lambda_c \bar{D}}^{1/2^-} C_{\Lambda_c \bar{D} \bar{p}, B_s}^{1/2^-}$	$0.25 - 1.48 i$	$-0.09 - 0.71 i$
$C_{\psi p, \Lambda_c \bar{D}^*}^{1/2^-} C_{\Lambda_c \bar{D}^* \bar{p}, B_s}^{1/2^-}$	$1.29 - 0.02 i$	$0.49 + 0.40 i$
$C_{\psi p, \Sigma_c \bar{D}}^{1/2^-} C_{\Sigma_c \bar{D} \bar{p}, B_s}^{1/2^-}$	$-0.99 - 1.99 i$	$1.33 - 4.54 i$
$C_{\text{dir}}^{1/2^-}$	$2.16 + 0.00 i$	$1.52 + 0.00 i$
$\Lambda$ (MeV)	1000	1000
$h_{\Lambda_c \bar{D}(1/2^-)}$	2.5	0
$h_{\Lambda_c \bar{D}^*(1/2^-)}$	2.5	0
$h_{\Sigma_c \bar{D}(1/2^-)}$	-2	0

$\Lambda_c^+ \bar{D}^0$ ,  $\Lambda_c^+ \bar{D}^{*0}$ , and  $\Sigma_c \bar{D}$  one-loop amplitudes create cusp structures near their thresholds. In particular, the  $\Sigma_c \bar{D}$  threshold cusp appearing slightly above the  $\Sigma_c \bar{D}$  threshold well describes the  $P_c(4337)^+$  peak structure. The cusp can mimic a  $1/2^-$  resonance contribution, which is consistent with one of possible  $P_c(4337)^+$  spin-parity assignments found in Ref. [65]. Thus, within our model,  $P_c(4337)^+$  does not exist as an exotic hadron.

Contributions from various mechanisms are plotted in Fig. 3(b); the  $Y_c \bar{D}^{(*)}$  single channel scattering amplitudes are implemented. The spectra are not smeared with the bin width. The blue dashed curve is from the coherently summed  $\Sigma_c \bar{D}$  and  $\bar{\Sigma}_c D$  one-loop amplitudes. The  $\Sigma_c \bar{D}$  and  $\bar{\Sigma}_c D$  one-loop amplitudes create a threshold cusp and a reflection (broad bump in  $M_{J/\psi p} = 4.1 - 4.2$  GeV), respectively, in the fairly separated  $M_{J/\psi p}$  regions. Due to the attractive  $\Sigma_c \bar{D}$  interaction, the threshold cusp is rather sharp. Similarly, the green dashed curve is from the  $\Lambda_c^+ \bar{D}^{*0}$  and  $\bar{\Lambda}_c D^{*0}$  one-loop amplitudes. The repulsive  $\Lambda_c^+ \bar{D}^{*0}$  interaction creates a less sharp threshold cusp. Meanwhile, the  $\Lambda_c^+ \bar{D}^0$  and  $\bar{\Lambda}_c D^0$  one-loop amplitudes significantly interfere with each other, and the  $\Lambda_c^+ \bar{D}^0$  threshold cusp does not appear as a peak structure (magenta dash-dotted curve).

The calculation is also compared with the  $M_{p \bar{p}}$  distribution data in Fig. 4(a). Although this observable is

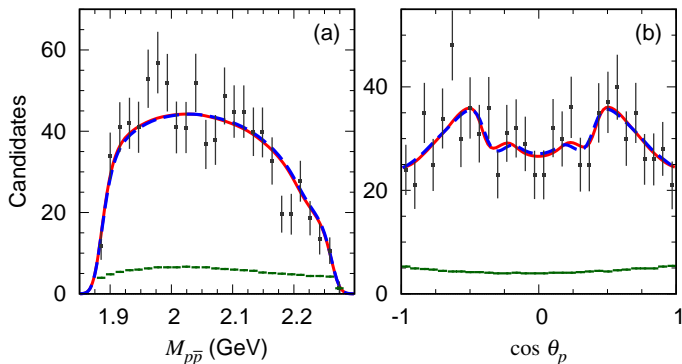


FIG. 4. (a)  $p\bar{p}$  invariant mass and (b) proton helicity angle distributions for  $B_s^0 \rightarrow J/\psi p\bar{p}$ . The other features are the same as Fig. 3.

not included in the fitting procedure, the agreement is reasonable.

Finally, a comparison is made for the proton helicity angle distribution data in Fig. 4(b). Remarkably, our model reproduces an oscillating behavior rather well. The  $\Sigma_c \bar{D}$  and  $\bar{\Sigma}_c D$  threshold cusps create the larger peaks at  $\cos \theta_p \sim \pm 0.5$ , and an interference with the  $\Lambda_c^+ \bar{D}^{*0}$  and  $\bar{\Lambda}_c D^{*0}$  threshold cusps causes the smaller peaks at  $\cos \theta_p \sim \pm 0.2$ . On the other hand, in the LHCb analysis [65], while the  $P_c(4337)^+$  and  $\bar{P}_c(4337)$  resonant mechanisms well reproduce the peaks at  $\cos \theta_p \sim \pm 0.5$ , their model's flat distribution in  $|\cos \theta_p| \lesssim 0.3$  is qualitatively different from the seemingly oscillating data. Yet, the LHCb's flat distribution is still consistent with the data within large errors. It is important to confirm the oscillating behavior with higher statistics data to discriminate different models.

We varied the common cutoff in the form factors over  $\Lambda = 0.8 - 2$  GeV, and refitted the parameters. The fit quality does not significantly change. This stability is expected since the singular behaviors of the threshold cusps do not sensitively depend on the cutoff.

Can we observe effects of the  $Y_c \bar{D}^{(*)}$  coupled-channel dynamics in the LHCb data? The red solid and blue dashed curves in Figs. 3(a) and 4 are rather similar. The fit quality does not significantly change as long as the  $Y_c \bar{D}^{(*)}$  scattering length is varied within a range where the sign does not change and neither a bound pole nor a virtual pole very close to the threshold appears. This indicates that the structures in the spectra are essentially caused by the kinematical effects, irrespective of the dynamical details. The result also partly supports our assumption that the complex couplings (fitting parameters) well absorb the  $Y_c \bar{D}^{(*)}$  coupled-channel effects that determine the magnitude and phase of each one-loop amplitude. Conversely, the  $Y_c \bar{D}^{(*)}$  coupled-channel effects may be extracted from the data only if we understand the initial weak vertices in advance. Thus, to address the question at the beginning of this paragraph, we need an experimental and/or lattice QCD determina-

tion of the initial weak vertices as well as higher statistics data for  $B_s^0 \rightarrow J/\psi p\bar{p}$ .

The  $P_c(4312)^+$  and  $P_c(4337)^+$  peaks appear in  $\Lambda_b^0 \rightarrow J/\psi p K^-$  and  $B_s^0 \rightarrow J/\psi p\bar{p}$ , respectively, but not vice versa or both. Considering (anomalous) threshold cusps, we can draw a consistent picture of this mutual exclusiveness as follows. As shown in Fig. 3, the  $P_c(4337)^+$  peak can be understood as the  $\Sigma_c \bar{D}$  threshold cusp. This may imply a comparable  $\Lambda_c^+ \bar{D}^{*0}$  threshold cusp, which is also supported by the oscillating  $\cos \theta_p$  distribution data in Fig. 4(b). In Refs. [66, 67], the  $P_c(4312)^+$  peak is explained by an interference between the  $\Lambda_c^+ \bar{D}^{*0}$  threshold cusp and an anomalous  $\Sigma_c \bar{D}$  threshold cusp due to the double-triangle diagram. Thus, the  $P_c(4312)^+$  and  $P_c(4337)^+$  peak structures are consequences of the different interference patterns of the (anomalous)  $\Sigma_c \bar{D}$  and  $\Lambda_c^+ \bar{D}^{*0}$  threshold cusps.

In Ref. [75], the authors discussed  $P_c(4312)^+$  and  $P_c(4337)^+$  as resonance or bound state poles from  $\Lambda_c^+ \bar{D}^{*0} - \Sigma_c^{(*)} \bar{D}$  coupled-channel dynamics. Within this picture, however, it is difficult to explain the above mutual exclusiveness of the  $P_c^+$ 's appearances. Another possibility discussed in the paper is that  $P_c(4337)^+$  is a  $\chi_{c0} p$  bound state (hadrocharmonium). However, a strongly attractive charmonium-nucleon interaction does not seem likely since lattice QCD calculations found rather weak  $J/\psi N$  and  $\eta_c N$  interactions [76, 77]. Also, this scenario implies that the strength of a weak  $B_s^0 \rightarrow \chi_{c0} p\bar{p}$  decay vertex would be significantly larger than that of  $B_s^0 \rightarrow J/\psi p\bar{p}$ ; this implication does not seem likely, either. As mentioned earlier, the weak  $B_s^0 \rightarrow J/\psi p\bar{p}$  decay vertex would play a minor role since the  $p\bar{p}$  threshold enhancement is absent; other  $B_s^0 \rightarrow$  charmonium +  $p\bar{p}$  are also expected to be minor. Thus, the scenarios discussed in Ref. [75] do not seem as comparably convincing as the one proposed in this work.

#### IV. SUMMARY

We developed a model to analyze the recent LHCb data on  $B_s^0 \rightarrow J/\psi p\bar{p}$ . The  $\Sigma_c \bar{D}$  one-loop mechanism in the model causes a threshold cusp that fits well the  $P_c(4337)^+$  peak in the  $J/\psi p$  invariant mass distribution data. We also showed that an oscillating behavior in the proton helicity angle distribution data can be understood as an interference between the  $\Sigma_c \bar{D}$  and  $\Lambda_c \bar{D}^*$  threshold cusps. Combining these results with our earlier analysis on  $\Lambda_b^0 \rightarrow J/\psi p K^-$ , we conclude that  $P_c(4312)^+$  in  $\Lambda_b^0 \rightarrow J/\psi p K^-$  and  $P_c(4337)^+$  in  $B_s^0 \rightarrow J/\psi p\bar{p}$  are due to different interference patterns between the  $\Sigma_c \bar{D}$  and  $\Lambda_c \bar{D}^*$  (anomalous) threshold cusps. In this way, we can consistently understand why the  $P_c(4312)^+$  and  $P_c(4337)^+$  peaks appear in  $\Lambda_b^0 \rightarrow J/\psi p K^-$  and  $B_s^0 \rightarrow J/\psi p\bar{p}$ , respectively, but not vice versa or both. The conclusion may also call for the reconsideration of the existing data that have been interpreted as exotic hadron signals.

## ACKNOWLEDGMENTS

We thank S. Sakai for useful discussions. We also acknowledge J. Haidenbauer for useful discussions on  $p\bar{p}$  threshold enhancements. This work is in part supported by National Natural Science Foundation of China (NSFC) under contracts U2032103 and 11625523,

and also by National Key Research and Development Program of China under Contracts 2020YFA0406400 (S.X.N.). The support is also from JSPS KAKENHI under Grant No. JP20K14478 (Y.Y.) and from Grants-in Aid for Scientific Research on Innovative Areas under Grant No. 18H05407 (A.H.).

- 
- [1] S.K. Choi et al. (Belle Collaboration), Observation of a narrow charmoniumlike state in exclusive  $B^\pm \rightarrow K^\pm \pi^+ \pi^- J/\psi$  decays, *Phys. Rev. Lett.* **91**, 262001 (2003).
- [2] H.-X. Chen, W. Chen, X. Liu, and S.-L. Zhu, The hidden-charm pentaquark and tetraquark states, *Phys. Rep.* **639**, 1 (2016).
- [3] A. Hosaka, T. Iijima, K. Miyabayashi, Y. Sakai, and S. Yasui, Exotic hadrons with heavy flavors:  $X$ ,  $Y$ ,  $Z$ , and related states, *PTEP* **2016**, 062C01 (2016).
- [4] R.F. Lebed, R.E. Mitchell, and E.S. Swanson, Heavy-Quark QCD Exotica, *Prog. Part. Nucl. Phys.* **93**, 143 (2017).
- [5] A. Esposito, A. Pilloni, and A.D. Polosa, Multiquark Resonances, *Phys. Rept.* **668**, 1 (2017).
- [6] A. Ali, J.S. Lange, and S. Stone, Exotics: Heavy Pentaquarks and Tetraquarks, *Prog. Part. Nucl. Phys.* **97**, 123 (2017).
- [7] F.-K. Guo, C. Hanhart, U.-G. Meißner, Q. Wang, Q. Zhao, and B.-S. Zou, Hadronic molecules, *Rev. Mod. Phys.* **90**, 015004 (2018).
- [8] S.L. Olsen, T. Skwarnicki, and D. Zieminska, Nonstandard heavy mesons and baryons: Experimental evidence, *Rev. Mod. Phys.* **90**, 015003 (2018).
- [9] N. Brambilla, S. Eidelman, C. Hanhart, A. Nefediev, C.-P. Shen, C.E. Thomas, A. Vairo, and C.-Z. Yuan, The  $XYZ$  states: Experimental and theoretical status and perspectives, *Phys. Rept.* **873**, 1 (2020).
- [10] M.-Z. Liu, Y.-W. Pan, F.-Z. Peng, M.S. Sánchez, L.-S. Geng, A. Hosaka, and M.P. Valderrama, Emergence of a complete heavy-quark spin symmetry multiplet: seven molecular pentaquarks in light of the latest LHCb analysis, *Phys. Rev. Lett.* **122**, 242001 (2019).
- [11] C.-W. Xiao, J. Nieves, and E. Oset, Heavy quark spin symmetric molecular states from  $\bar{D}^{(*)}\Sigma_c^{(*)}$  and other coupled channels in the light of the recent LHCb pentaquarks, *Phys. Rev. D* **100**, 014021 (2019).
- [12] C.-J. Xiao, Y. Huang, Y.-B. Dong, L.-S. Geng, and D.-Y. Chen, Exploring the molecular scenario of  $P_c(4312)$ ,  $P_c(4440)$ , and  $P_c(4457)$ , *Phys. Rev. D* **100**, 014022 (2019).
- [13] Z.-H. Guo and J.A. Oller, Anatomy of the newly observed hidden-charm pentaquark states:  $P_c(4312)$ ,  $P_c(4440)$ , and  $P_c(4457)$ , *Phys. Lett. B* **793**, 144 (2019).
- [14] J. He, Study of  $P_c(4457)$ ,  $P_c(4440)$ , and  $P_c(4312)$  in a quasipotential Bethe-Salpeter equation approach, *Eur. Phys. J. C* **79**, 393 (2019).
- [15] F.-K. Guo, H.-J. Jing, U.-G. Meißner, and S. Sakai, Isospin breaking decays as a diagnosis of the hadronic molecular structure of the  $P_c(4457)$ , *Phys. Rev. D* **99**, 091501(R) (2019).
- [16] H.-X. Chen, W. Chen, and S.-L. Zhu, Possible interpretations of the  $P_c(4312)$ ,  $P_c(4440)$ , and  $P_c(4457)$ , *Phys. Rev. D* **100**, 051501(R) (2019).
- [17] R. Chen, Z.-F. Sun, X. Liu, and S.-L. Zhu, Strong LHCb evidence supporting the existence of the hidden-charm molecular pentaquarks, *Phys. Rev. D* **100**, 011502(R) (2019).
- [18] G.-J. Wang, L.-Y. Xiao, R. Chen, X.-H. Liu, X. Liu, and S.-L. Zhu, Probing hidden-charm decay properties of  $P_c$  states in a molecular scenario, *Phys. Rev. D* **102**, 036012 (2020).
- [19] T. Gutsche and V.E. Lyubovitskij, Structure and decays of hidden heavy pentaquarks, *Phys. Rev. D* **100**, 094031 (2019).
- [20] B. Wang, L. Meng, and S.-L. Zhu, Hidden-charm and hidden-bottom molecular pentaquarks in chiral effective field theory, *JHEP* **11**, 108 (2019).
- [21] J. He and D.-Y. Chen, Molecular states from  $\Sigma_c^{(*)}\bar{D}^{(*)}-\Lambda_c\bar{D}^{(*)}$  interaction, *Eur. Phys. J. C* **79**, 887 (2019).
- [22] Y.-H. Lin and B.-S. Zou, Strong decays of the latest LHCb pentaquark candidates in hadronic molecule pictures, *Phys. Rev. D* **100**, 056005 (2019).
- [23] T.J. Burns and E.S. Swanson, Molecular interpretation of the  $P_c(4440)$  and  $P_c(4457)$  states, *Phys. Rev. D* **100**, 114033 (2019).
- [24] Y.-J. Xu, C.-Y. Cui, Y.-L. Liu, and M.-Q. Huang, Partial decay widths of  $P_c(4312)$  as a  $\bar{D}\Sigma_c$  molecular state, *Phys. Rev. D* **102**, 034028 (2020).
- [25] Y. Yamaguchi, H. García-Tecocoatzi, A. Giachino, A. Hosaka, E. Santopinto, S. Takeuchi, and M. Takizawa,  $P_c$  pentaquarks with chiral tensor and quark dynamics, *Phys. Rev. D* **101**, 091502(R) (2020).
- [26] S. Sakai, H.-J. Jing, and F.-K. Guo, Decays of  $P_c$  into  $J/\psi N$  and  $\eta_c N$  with heavy quark spin symmetry, *Phys. Rev. D* **100**, 074007 (2019).
- [27] M.B. Voloshin, Some decay properties of hidden-charm pentaquarks as baryon-meson molecules, *Phys. Rev. D* **100**, 034020 (2019).
- [28] Q. Wu and D.-Y. Chen, Production of  $P_c$  states from  $\Lambda_b$  decay, *Phys. Rev. D* **100**, 114002 (2019).
- [29] J.-R. Zhang, Exploring a  $\Sigma_c\bar{D}$  state: with focus on  $P_c(4312)^+$ , *Eur. Phys. J. C* **79**, 1001 (2019).
- [30] H. Xu, Q. Li, C.-H. Chang, and G.-L. Wang, Recently observed  $P_c$  as molecular states and possible mixture of  $P_c(4457)$ , *Phys. Rev. D* **101**, 054037 (2020).
- [31] M.-L. Du, V. Baru, F.-K. Guo, C. Hanhart, U.-G. Meißner, J.A. Oller, and Q. Wang, Interpretation of the LHCb  $P_c$  states as hadronic molecules and hints of a narrow  $P_c(4380)$ , *Phys. Rev. Lett.* **124**, 072001 (2020).
- [32] M.-L. Du, V. Baru, F.-K. Guo, C. Hanhart, U.-G. Meißner, J.A. Oller, and Q. Wang, Revisiting the nature

- of the  $P_c$  pentaquarks, JHEP **08**, 157 (2021).
- [33] C.-W. Xiao, J.-X. Lu, J.-J. Wu, and L.-S. Geng, How to reveal the nature of three or more pentaquark states, Phys. Rev. D **102**, 056018 (2020).
- [34] P. Ling, X.-H. Dai, M.-L. Du, and Q. Wang, Prompt production of the hidden charm pentaquarks in the LHC, Eur. Phys. J. C **81**, 819 (2021).
- [35] X.-Z. Ling, J.-X. Lu, M.-Z. Liu, and L.-S. Geng,  $P_c(4457) \rightarrow P_c(4312)\pi/\gamma$  in the molecular picture, Phys. Rev. D **104**, 074022 (2021).
- [36] M.-W. Li, Z.-W. Liu, Z.-F. Sun, and R. Chen, Magnetic moments and transition magnetic moments of  $P_c$  and  $P_{cs}$  states, Phys. Rev. D **104**, 054016 (2021).
- [37] K. Azizi, Y. Sarac, and H. Sundu, Properties of the  $P_c(4312)$  pentaquark and its bottom partner, Chin. Phys. C **45**, 053103 (2021).
- [38] Y. Yamaguchi, A. Giachino, A. Hosaka, E. Santopinto, S. Takeuchi and M. Takizawa, Hidden-charm and bottom meson-baryon molecules coupled with five-quark states, Phys. Rev. D **96**, 114031 (2017).
- [39] Y. Yamaguchi and E. Santopinto, Hidden-charm pentaquarks as a meson-baryon molecule with coupled channels for  $\bar{D}^{(*)}\Lambda_c$  and  $\bar{D}^{(*)}\Sigma_c^{(*)}$ , Phys. Rev. D **96**, 014018 (2017).
- [40] A. Ali and A.Ya. Parkhomenko, Interpretation of the narrow  $J/\psi p$  peaks in  $\Lambda_b \rightarrow J/\psi p K^-$  decay in the compact diquark model, Phys. Lett. B **793**, 365 (2019).
- [41] A. Pimikov, H.-J. Lee, and P. Zhang, Hidden charm pentaquarks with color-octet substructure in QCD Sum Rules, Phys. Rev. D **101**, 014002 (2020).
- [42] Z.-G. Wang, Analysis of the  $P_c(4312)$ ,  $P_c(4440)$ ,  $P_c(4457)$  and related hidden-charm pentaquark states with QCD sum rules, Int. J. Mod. Phys. A **35**, 2050003 (2020).
- [43] R. Zhu, X. Liu, H. Huang, and C.-F. Qiao, Analyzing doubly heavy tetra- and penta-quark states by variational method, Phys. Lett. B **797**, 134869 (2019).
- [44] X.-Z. Weng, X.-L. Chen, W.-Z. Deng, and S.-L. Zhu, Hidden-charm pentaquarks and  $P_c$  states, Phys. Rev. D **100**, 016014 (2019).
- [45] F. Giannuzzi, Heavy pentaquark spectroscopy in the diquark model, Phys. Rev. D **99**, 094006 (2019).
- [46] F. Stancu, Spectrum of the  $uudc\bar{c}$  hidden charm pentaquark with an SU(4) flavor-spin hyperfine interaction, Eur. Phys. J. C **79**, 957 (2019).
- [47] Y. Dong, P. Shen, F. Huang, and Z. Zhang, Selected strong decays of pentaquark State  $P_c(4312)$  in a chiral constituent quark model, Eur. Phys. J. C **80**, 341 (2020).
- [48] E. Santopinto and A. Giachino, Compact pentaquark structures, Phys. Rev. D **96**, 014014 (2017).
- [49] J. Ferretti, E. Santopinto, M.N. Anwar, and M.A. Bedolla, The baryo-quarkonium picture for hidden-charm and bottom pentaquarks and LHCb  $P_c(4380)$  and  $P_c(4450)$  states, Phys. Lett. B **789**, 562 (2019).
- [50] J. Ferretti and E. Santopinto, Hidden-charm and bottom tetra- and pentaquarks with strangeness in the hadro-quarkonium and compact tetraquark models, JHEP **04**, 119 (2020).
- [51] M.I. Eides, V.Yu Petrov, and M.V. Polyakov, New LHCb pentaquarks as hadrocharmonium states, Mod. Phys. Lett. A **35**, 2050151 (2020).
- [52] F.-K. Guo, X.-H. Liu, and S. Sakai, Threshold cusps and triangle singularities in hadronic reactions, Prog. Part. Nucl. Phys. **112**, 103757 (2020).
- [53] P.A. Zyla et al. (Particle Data Group), The Review of Particle Physics, Prog. Theor. Exp. Phys. **2020**, 083C01 (2020).
- [54] R. Aaij et al. (LHCb Collaboration), Observation of  $J/\psi p$  resonances consistent with pentaquark states in  $\Lambda_b^0 \rightarrow J/\psi p K^-$  decays, Phys. Rev. Lett. **115**, 072001 (2015).
- [55] R. Aaij et al. (LHCb Collaboration), Observation of a Narrow Pentaquark State,  $P_c(4312)^+$ , and of the Two-Peak Structure of the  $P_c(4450)^+$ , Phys. Rev. Lett. **122**, 222001 (2019).
- [56] Q. Wang, X.-H. Liu, and Q. Zhao, Photoproduction of hidden charm pentaquark states  $P_c^+(4380)$  and  $P_c^+(4450)$ , Phys. Rev. D **92**, 034022 (2015).
- [57] V. Kubarovsky and M.B. Voloshin, Formation of hidden-charm penta quarks in photon-nucleon collisions, Phys. Rev. D **92**, 031502(R) (2015).
- [58] M. Karliner and J.L. Rosner, Photoproduction of Exotic Baryon Resonances, Phys. Lett. B **752**, 329 (2016).
- [59] A.N. Hiller Blin, C. Fernández-Ramírez, A. Jackura, V. Mathieu, V.I. Mokeev, A. Pilloni, and A.P. Szczepaniak, Studying the  $P_c(4450)$  resonance in  $J/\psi$  photoproduction off protons, Phys. Rev. D **94**, 034002 (2016).
- [60] X.-Y. Wang, X.-R. Chen, and J. He, Possibility to study pentaquark states  $P_c(4312)$ ,  $P_c(4440)$ , and  $P_c(4457)$  in  $\gamma p \rightarrow J/\psi p$  reaction, Phys. Rev. D **99**, 114007 (2019).
- [61] J.-J. Wu, T.-S.H. Lee, and B.-S. Zou, Nucleon resonances with hidden charm in  $\gamma p$  reactions, Phys. Rev. C **100**, 035206 (2019).
- [62] X. Cao and J.-P. Dai, Confronting pentaquark photoproduction with new LHCb observations, Phys. Rev. D **100**, 054033 (2019).
- [63] A. Ali et al. (GlueX Collaboration), First measurement of near-threshold  $J/\psi$  exclusive photoproduction off the proton, Phys. Rev. Lett. **123**, 072001 (2019).
- [64] R. Aaij et al. (LHCb Collaboration), Evidence for exotic hadron contributions to  $\Lambda_b^0 \rightarrow J/\psi p \pi^-$  decays, Phys. Rev. Lett. **117**, 082003 (2016).
- [65] R. Aaij et al. (LHCb collaboration), Evidence for a new structure in the  $J/\psi p$  and  $J/\psi \bar{p}$  systems in  $B_s^0 \rightarrow J/\psi p \bar{p}$  decays, arXiv:2108.04720.
- [66] S.X. Nakamura,  $P_c(4312)^+$ ,  $P_c(4380)^+$ , and  $P_c(4457)^+$  as double triangle cusps, Phys. Rev. D **103**, L111503 (2021).
- [67] S.X. Nakamura, Novel description of  $P_c(4312)^+$ ,  $P_c(4380)^+$ , and  $P_c(4457)^+$  with double triangle cusps, PoS CHARM2020, 029 (2021).
- [68] D.-Y. Chen and X. Liu,  $Z_b(10610)$  and  $Z_b(10650)$  structures produced by the initial single pion emission in the  $\Upsilon(5S)$  decays, Phys. Rev. D **84**, 094003 (2011).
- [69] D.-Y. Chen, X. Liu, and T. Matsuki, Reproducing the  $Z_c(3900)$  structure through the initial-single-pion-emission mechanism, Phys. Rev. D **88**, 036008 (2013).
- [70] R. Aaij et al. (LHCb collaboration), Observation of  $B_{(s)}^0 \rightarrow J/\psi p \bar{p}$  decays and precision measurements of the  $B_{(s)}^0$  masses, Phys. Rev. Lett. **122**, 191804 (2019).
- [71] A. Sibirtsev, J. Haidenbauer, S. Krewald, U.-G. Meißner, and A.W. Thomas, Near threshold enhancement of the  $p \bar{p}$  mass spectrum in  $J/\Psi$  decay, Phys. Rev. D **71**, 054010 (2005).
- [72] X.-W. Kang, J. Haidenbauer, and U.-G. Meißner, Near-threshold  $p \bar{p}$  invariant mass spectrum measured in  $J/\psi$  and  $\psi'$  decays, Phys. Rev. D **91**, 074003 (2015).

- [73] X.-K. Dong, F.-K. Guo, and B.-S. Zou, Explaining the Many Threshold Structures in the Heavy-Quark Hadron Spectrum, *Phys. Rev. Lett.* **126**, 152001 (2021).
- [74] H. Kamano, S.X. Nakamura, T.-S.H. Lee, and T. Sato, Unitary coupled-channels model for three-mesons decays of heavy mesons, *Phys. Rev. D* **84**, 114019 (2011).
- [75] M.-J. Yan, F.-Z. Peng, M.S. Sánchez, and M.P. Valderama, Interpretations of the new LHCb  $P_c(4337)^+$  pentaquark state, arXiv:2108.05306.
- [76] U. Skerbis and S. Prelovsek, Nucleon- $J/\psi$  and nucleon- $\eta_c$  scattering in  $P_c$  pentaquark channels from LQCD, *Phys. Rev. D* **99**, 094505 (2019).
- [77] T. Sugiura, Y. Ikeda, and N. Ishii, Charmonium-nucleon interactions from 2+1 flavor lattice QCD, PoS LATTICE2018 (2019) 093.